2024 14th Workshop on Hyperspectral Imaging and Signal Processing: Evolution in Remote Sensing (WHISPERS) | 979-8-3315-1313-9/24/$31.00 ©2024 IEEE | DOI: 10.1109/WHISPERS65427.2024.10876513

MULTISPECTRAL SNAPSHOT MICROSCOPY AS AN EXPOSURE ASSESSMENT TOOL

*Carolina Blanch-Perez-del-Notario**[a], *Amir Asadollahi*[a], *Pieter Bertier*[b], *Murali Jayapala*[a]

[a]imec, Kapeldreef 75, Leuven, 3001, Belgium; [b]Belgian Center for Occupational Hygiene, BeCOH, Brusselsesteenweg 46, 3000 Leuven, Belgium

ABSTRACT

Hyperspectral imaging in combination with microscopy can increase material discrimination possibilities with respect to regular microscopy imaging. We explore this discrimination potential to assess exposure to particle contamination. We focus on discriminating health relevant particles such as silica, in the respirable size fraction. To do so, multispectral imaging in combination with transmission microscopy is used for particle material identification. We use two compact snapshots near-infrared (NIR) cameras providing 16-25 spectral bands in the 600-960 nm range. The multispectral microscopy system has been tested for discrimination of silica among fourteen different particle materials. The analysis performed shows potential to accurately discriminate the 14 tested particle materials. In addition, the band relevance analysis shows that only a few specific bands are needed to provide accurate discrimination. The multispectral method presented could therefore enable a faster exposure assessment than traditional techniques for occupational exposure estimation.

Index Terms— Multispectral, portable microscopy, respirable particles, silica.

1. INTRODUCTION

Crystalline silica or quartz (SiO2) is the most widely occurring of all minerals and it is found in most rocks. In the dry form, fine crystalline silica constitutes a toxic hazard since its inhalation as airborne dust could give rise to silicosis [1]. Silica is encountered during many industrial processes which use minerals e.g. construction, quarrying and mining, brick, tile and refractory manufacture, pottery and ceramic, sandblasting, glass manufacture. Exposure to crystalline silica or quartz can also be linked to immune system related diseases [2]. For this reason, workers' exposure to silica particles is monitored by occupational hygienists who focus on the fraction of respirable (smaller than 15 microns) crystalline silica particle [3] that can cause significant lung damage. There are currently several standardized sampling and analysis techniques from environmental and occupational hygienists to assess the exposure to silica particles. Aerosol samples are typically collected on filter substrates by size selective cyclones or foams and analyzed for their crystalline silica content in the laboratory by X-Ray Diffraction (XRD) or Fourier Transform Infra-Red (FTIR). The latter are also the only two methods that are standardized for that purpose [4]. XRD is a non-destructive technique that provides detailed information about the crystallographic structure, chemical composition, and physical properties of a material [5]. FTIR [6] identifies chemical bonds in a molecule by producing an infrared absorption or reflection spectrum that can indicate the components present. Other methods are mostly used for research purposes. Scanning electron microscopy [7] (SEM) or laser diffraction are laboratory methods that are often used for determining the particle sizes of dust deposits. These methods only give information on particle size, not composition. For measurement of particle sizes of aerosols at the workplace, optical particle sizers, aerodynamic particle sizers, condensation particle counters or aerosol mobility spectrometers [8] are used. Phase contrast microscopy (PCM) and SEM/TEM+EDS (Transmission Electron Microscopy with Energy-dispersive X-ray Spectroscopy) are standardized methods used in occupational hygiene projects for identification and elemental characterization on non-fibrous particulate matter, but it is a labor- and cost intensive method. XRD, FTIR, laser diffraction particle sizing, SEM/TEM and PCM are laboratory methods, with typical turnaround times of several weeks, therefore the results are not directly available to the occupational hygienist during the sampling campaigns. The National Institute for Occupational Safety and Health (NIOSH) has developed an FTIR method for analyzing the respirable crystalline silica content of aerosol samples collected on filter substrates at the workplace by means of a portable FTIR spectrometer and a purpose designed software [9]. This method offers the substantial advantage of providing the exposure data immediately after sampling ('end-of-shift' measurement). Yet, it requires an extensive database of measurement data from laboratory methods to deal with spectral interferences from other minerals. That data is available for the coal mining industry, for which the method was initially developed, but not for other industries.

This paper presents the use of Hyperspectral Imaging Systems (HSI) in combination with microscopy for the identification of hazardous substances in workplace dust samples. Hyperspectral imaging provides an image with both

spatial and spectral information providing insights in the chemical composition of materials with their spatial distribution [10], with its key advantages being that it is a non-invasive, non-contact and non-destructive technology. Both HSI and FT-IR methods can obtain reflectance or transmittance spectra in IR of the dust deposits. The key differences are in their limitations with respect to time, area coverage, and spectral range. In FT-IR each measurement is a single point spectrum, so inspecting a wider area is more time consuming. Hyperspectral imaging, instead, produces spectra of a full image and it can therefore cover larger areas in less time (few minutes for linescan systems [11], below a second for snapshot camera systems [12]). In addition, FT-IR imaging systems are highly complex and expensive (~200 k€) [13]. FT-IR spectra often cover the 2500-25000 nm range while HSI focuses on a smaller range, typically visible (400–700 nm) and the near infrared (from 700 nm up to 2500 nm). There are many applications where hyperspectral imaging has gained high interest in recent years [14]. For instance, in ore, mineral and oil gas industries where hyperspectral core logging is becoming a routine process. Some authors have used hyperspectral imaging in the VNIR range (400-1000 nm) in combination with deep learning to identify minerals such as hematite, galena, and chalcopyrite in an ore [15]. Different hematite grain sizes are considered, from below 20 µm up to 1 cm and classification accuracies around 90% are obtained, in comparison with 30% for color imaging. Similarly, hyperspectral imaging in the LWIR range (7.7 to 11.8 µm) has been used to accurately discriminate 21 different mineral powders, such as silica, and 3 mixes of them [16]. Grain size ranges from 12 µm up to around 600 µm are considered. Both SWIR (1000-2500 nm) and LWIR (7.5 to 11.5 µm) imaging have been evaluated for detection of clay minerals in sand [17]. Prediction of quartz and clay contents could be accurately done and compared with more expensive and time-consuming reference methods. All this work focuses on inspection of bulk mineral samples or particle aggregations and does not address single particle inspection. Single particle inspection requires the combination of microscopy and hyperspectral imaging. In this context, dark field hyperspectral microscopy has been used in the 400-1000 nm range to detect nano particles in biological tissues [18]. Finally, a high-throughput spectroscopy and microscopy imaging system has been proposed for characterization of gold nano particles at the single-particle level [19], enabling a single snapshot image of 1024x1024 pixels at high temporal resolution (26 fps) in the visual range of 400-700 nm. The developed method enables quantification of spectra and spatial information. Only gold nanoparticle detection is addressed among 2 or 3 different material types. Our work also focuses on mineral particle discrimination with fast acquisition multispectral snapshot imaging but for bright-field imaging. In our previous work [20], we explored the use of hyperspectral cameras of 150 bands in the VNIR range to target 15 particle materials of respirable size (~ 5 µm), with focus on health-relevant particles such as silica. Now we extend this study to multispectral snapshot cameras [12], which offer a reduced spatial and spectral resolution (16-25 bands) but enable faster inspection and increased portability for on-site measurements.

2. MATERIALS AND METHODS

For the particle material selection, health-relevant materials like silica are included, together with potential confounders particles, such as barite. By confounder, we mean particles that could be present in the same sampling environment and be similar enough to be misclassified by silica, which is the target material. A set of 15 different material particle powders was prepared including quartz (the most common polymorph of crystalline silica). The particle types and its grain-size distribution are shown in [20], with a mean particle size in the order of 5 µm. The focus is to detect and discriminate silica particles, and specifically those at respirable size (below 15 microns), since those can penetrate deeper in the lungs and may propagate via blood to other organs in the body. The particle samples were deposited onto glass slides according to the defined particle sampling protocol [20], meant to be a pragmatical and simple approach to test for particle exposure in dust deposits covering surfaces at workplaces. Regular microscopy glass slides were used together with a tesa double-side tape that showed better adhesive properties for particles. In [20], a high spatial and spectral resolution camera was used with 150 bands and 7 Mpx resolution in the VNIR range (460-900 nm). The band relevance analysis showed that 3 bands, namely 643, 718, and 871 nm were sufficient to provide high classification accuracy. For this reason, we focus in this paper on multispectral snapshot cameras in the 600-950 nm range. In this respect, snapshot systems trade-off spectral and spatial resolution to provide much faster acquisition than scanning systems and better avoid any motion artifact. Figure 1 shows such a snapshot camera coupled to a Leica transmission microscope [21]. We test two snapshot cameras, described in [12], the first (RedNIR) with 16 bands over the 600-860 nm range, and 512x256 pixels resolution and a second one (NIR) with 25 bands in the 660-960 nm range and a 409x216 pixel resolution. A 20x and a 40x magnification objective are used respectively for the RedNIR and NIR cameras in combination with bright field imaging with a broadband tungsten-halogen light source. While the snapshot multispectral camera is a lower cost, compact and portable device, the transmission microscope is still bulky and expensive. To enable a truly cost-efficient and portable system, we tested our in-development portable microscope. Its schematic is shown in Figure 2. The light source used is a Quartz Tungsten-Halogen bulb with a color temperature of 2800K covering the full camera spectral range.

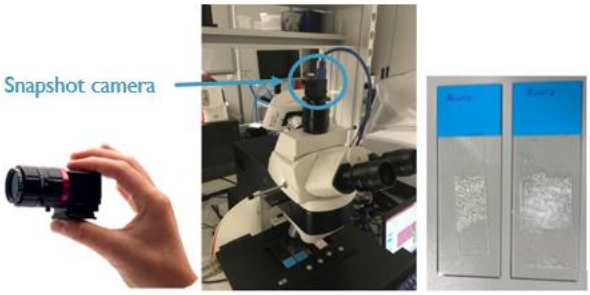

Figure 1: Snapshot camera (left) on microscope (middle), and example of glass slides samples (right).

The imaging part includes a 20X infinity-corrected Plan Achromatic objective lens with a 0.4 numerical aperture and working distance of 1.2 mm, mounted on a Z-axis translation stage. The Z-axis translation stage allows for precise fine focus adjustments and an electronically controllable optical shutter allows capture of dark reference images. The dimensions of the portable microscope are 40.7 cm in length and a width of 12 cm at the acrylic plate that holds the samples. The snapshot camera is shown at the opposite end of the light source, achieving a fully compact, cost-efficient, and portable system. Further developments are on-going, such as the addition of an XY translation stage or the inclusion of a higher magnification 40X objective lens.

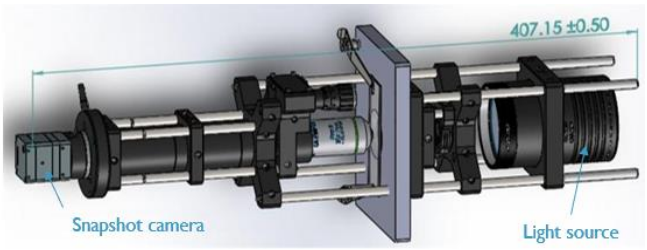

Figure 2: Schematics of portable microscope system.

In terms of processing pipeline, in our previous work [20], we used spectral means and median filtering to deal with the high within-particle spectral variation and improve classification performance. In the case of the snapshot cameras, the spatial resolution is considerably lower than the Snapscan camera [20], providing now a more averaged spectral mean per pixel. Therefore, applying median filtering [23] over each 5x5 block suffices. The classifiers tested, Quadratic Discriminant Classifier (QDC) [24] and Random Forest (RF) [25] are implemented with PerClass software [25] in combination with Matlab processing software [22]. These are pixel-based classifiers with no spatial information used to support classification. The training set consists of 30% pixels and the remaining pixels are used for testing. In addition, to find the most discriminative bands in our wavelength range, an in-house developed Genetic Algorithm [20], [26] in combination with the pixel classifier is used. The algorithm aim is to find a near-optimal subset of bands providing the highest mean classification accuracy in the test set. The behavior of the Genetic Algorithm is summarized in [20].

3. RESULTS AND DISCUSSION

Table 1 compares the mean performance (averaged over all materials) but also the minimum material accuracy for the different camera/classifier combinations. Higher accuracy is obtained with the NIR snapshot (660-960 nm) than with the RedNIR (600-860 nm), possibly due to the slightly different spectral range. In terms of classifiers, Random Forest outperforms the Quadratic classifier. With best performing settings, the lowest accuracy per material is still above 50%. From the models obtained, we can separate the particle materials into two groups. One first group with 8 target materials: quartz, barite (its main confounder), rutile, coal, feldspar, hematite, phlogopite and smectite, which are generally classified with high accuracy (>50%), while the second group (gypsum, calcite, dolomite, gibbsite, muscovite and kaolinite) suffer from considerably lower accuracy and are often miss-classified with each other but not with those of the first group. A potential classification model could then focus on the first group, providing high detection accuracy on the target component quartz/silica and 7 others. This model accuracy is given in the right-most column in Table 1, showing improved performance.

Table 1: Mean/min pixel accuracy of RedNIR & NIR

Camera	Classif	Mean/Min(all)	Mean/Min (8)
RedNIR 600-860nm	QDC	58.9%/13.6%	74.7% /23.3%
	RF	67.0%/30.4%	81.7% /45.7%
NIR5x5 660-950 nm	QDC	76.3%/ 53.7%	87.4%/ 67.3%
	RF	78.3%/ 47.0%	89.6%/73.8%

Additionally, quartz material gets typically classified with more than 90% accuracy (NIR), or 65% (RedNIR), with low percentage of quartz being misclassified only as barite. No other material causes misclassification with quartz. Note that at object level (particle level) a pixel majority vote can be used. Therefore, even a 65% accurate pixel classification would translate into noticeably higher classification accuracy at particle level. To visualize this, Figure 3 shows a few classified images for selected particles of several material samples such as Barite, Calcite, Gibbsite or Quartz. A few highlighted particles are manually selected to show the feasibility of spectral discrimination. We can see how the classifier attaches at pixel label the correct labels to the different particle types. In the case of quartz, only a small particle is misclassified as Barite. Table 2 shows the most relevant bands extracted from the Genetic Algorithm and the initial set of 16 bands (RedNIR) or 25 bands (NIR snapshot).

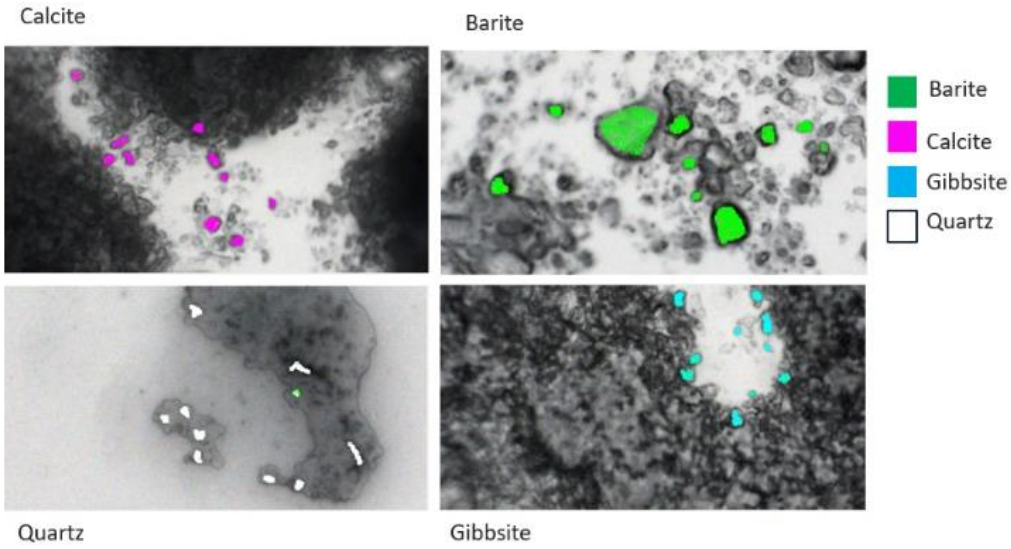

Figure 3: Classification images for some materials.

The classifier is for the full particle material set and the accuracy is shown for all particles and for the 8 target materials considered. The classification accuracies provided refer again to pixel accuracies, therefore with majority-vote at object level higher accuracy can be obtained.

Table 2: Mean/Min pixel accuracies for best band subsets of snapshot cameras, RF, mf5x5, considering all materials or the subset of 8.

# of Bands	Bands (nm)	Mean Min
Best 5 NIR all	685-847-894-907-945	69.0% 34.2%
Best 4 NIR all	685-847-916-945	65.9% 24.9%
Best 3 NIR all	667-847-907	63.0% 28.2%
Best 5 NIR (8)	685-847-894-907-945	83.9% 65.7%
Best 4 NIR (8)	685-847-916-945	82.5% 64.8%
Best 3 NIR (8)	667-847-907	78.5% 53.3%
Best 5 RNIR all	609-647-717-770 833	58.5% 19.8%
Best 4 RNIR all	647-699-735-833	56.3% 17.8%
Best 3 RNIR all	647-717-849	54.1% 12.4%
Best 5 RNIR (8)	609-647-717-770 833	76.3% 45.7%
Best 4 RNIR (8)	647-699-735-833	75.4% 30.5%
Best 3 RNIR (8)	647-717-849	74.8% 26.8%

As we can see, in practice, a lower set of bands is sufficient to achieve good discrimination. The algorithm selects a relatively even distribution of bands along the wavelength range. Bands in the additional 850-950 nm range provided by the NIR camera are selected as well, confirming the higher discrimination of this camera range. For the NIR camera (650-950 nm), 3 bands out of the 25 are sufficient to achieve good discrimination, while in the RedNIR camera (600-850 nm), a set of 5 bands is required to obtain similar performance. Identifying the most relevant bands can enable future application-specific custom sensor developments. In addition, initial tests performed with the portable microscope in combination with the snapshot NIR camera show potential for material discrimination as well. Figure 4 shows the spectral signature of 5 different materials acquired with the Portable microscopy system, where a mean classification accuracy of 90% is achieved for discrimination between those 5 materials with random forest classifier. Future work will extend the validation of the final version of current portable microscope in combination with the snapshot cameras and will consider a more extended set of materials.

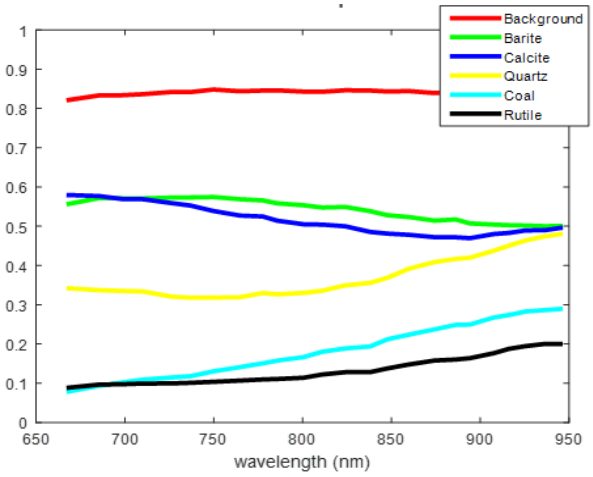

Figure 4: Mean reflectance spectra of portable multispectral system.

4. CONCLUSION

This paper has shown the potential of multispectral microscopy imaging for particle discrimination as a fast, cost-efficient, and portable exposure assessment method. The focus has been on identification of health relevant respirable size particles (around 5 µm), such as silica, discriminating them from other particle materials. The results show that high pixel classification accuracies (over 80%) can be obtained, and that a few bands (3 to 5) may be sufficient to achieve this. The preliminary tests with the portable microscope indicate as well that particle material discrimination could be feasible with a portable multispectral system.

ACKNOWLEDGMENTS

We want to acknowledge the Eximious project (European Union's Horizon 2020 research and innovation programme under grant agreement No 874707), for which this research has been done. We also want to thank Rieko Adriaens and Bart Aerts for their help in the particle sample preparation.

5. REFERENCES

[1] Mlika M, Adigun R, Bhutta BS. "Silica-Induced Pneumoconiosis." 2023 Feb 9. In: StatPearls [Internet]. Treasure Island (FL): StatPearls Publishing; 2023 Jan–. PMID: 30726026.

[2] Mapping Exposure-Induced Immune Effects: Connecting the Exposome and the Immunome | EXIMIOUS Project | Fact Sheet | H2020 | CORDIS | European Commission n.d. https://cordis.europa.eu/project/id/874707 (accessed July 7, 2024).

[3] "Health based particle-size-selective sampling", Application Note ITI-050. Available at https://tsi.com/getmedia/c388c1e7-9ab4-4f88-9f76-f2a3b64ba293/ITI-050?ext=.pdf

[4] ISO 16258, EN 17289 "Characterization of bulk materials – Determination of a size-weighted fine fraction and crystalline silica content – Part 1: General information and choice of tests methods", European Standard EN 17289-1.

[5] ISO 16258:2015 - Workplace air - Analysis of respirable crystalline silica by X-ray diffraction

[6] ISO 19087:2018 - Workplace air — Analysis of respirable crystalline silica by Fourier-Transform Infrared spectroscopy

[7] Wijnand Eduard et al, Content of clinker and other materials in personal thoracic aerosol samples from cement plants estimated by scanning electron microscopy and energy-dispersive X-ray microanalysis, Annals of Work Exposures and Health, Volume 67, (2023), p 990–1003, https://doi.org/10.1093/annweh/wxad047

[8] Evanly Vo et al, Performance Comparison of Field Portable Instruments to the Scanning Mobility Particle Sizer Using Monodispersed and Polydispersed Sodium Chloride Aerosols, Annals of Work Exposures and Health, Volume 62, Issue 6, (2018), Pages 711–720, https://doi.org/10.1093/annweh/wxy036

[9] Taekhee Lee, et al, "Respirable size-selective sampler for end-of-shift quartz measurement: Development and performance", in Journal of Occupational and Environmental Hygiene, vol 14, 5, pp 335-342, 2017. https://doi.org/10.1080/15459624.2016.1252845

[10] Kamruzzaman M., ... & Allen P. "Non-destructive prediction and visualization of chemical composition in lamb meat using NIR hyperspectral imaging and multivariate regression". Innov. Food Science and Emerging Technologies vol 16 (2012), pp 218-226.

[11] Pichette, J., Charle, W., & Lambrechts, A. Fast and compact internal scanning CMOS-based hyperspectral camera: the Snapscan. In Photonic Instrumentation Engineering IV (Vol. 10110, p. 1011014). International Society for Optics and Photonics, (2017).

[12] Blanch, C., Geelen, B., et al. "Compact high-speed snapshot multispectral imagers in the VIS/NIR (460-960 nm) and SWIR range (1.1-1.65 nm) and its potential in a diverse range of applications", in Hyperspectral Imaging and Applications II (Vol. 12338, pp. 11-24). SPIE, 2023.

[13] Primpke S, Christiansen SH, et al. Critical Assessment of Analytical Methods for the Harmonized and Cost-Efficient Analysis of Microplastics. Applied Spectroscopy. 2020; 74(9):1012–47. https://doi.org/10.1177/0003702820921465

[14] Khan, M. J., Khan, H.S et al. "Modern trends in hyperspectral image analysis: a review". IEEE Access Open Access Journal, DOI 10.1109/ACCESS.2018.2812999, March 2018.

[15] Okada, N., et al. (2020). Automated identification of mineral types and grain size using hyperspectral imaging and deep learning for mineral processing. Minerals, 10(9), 809.

[16] Myers, T. L., et al (2019). Hyperspectral imaging of minerals in the longwave infrared: the use of laboratory directional-hemispherical reference measurements for field exploration data. Journal of Applied Remote Sensing, 13(3), 034527-034527.

[17] Entezari, I., et al. (2017). Predicting the abundance of clays and quartz in oil sands using hyperspectral measurements. International journal of applied earth observation and geoinformation, 59, 1-8.

[18] Fakhrullin, R., et al (2021) "Dark field/hyperspectral microscopy for detecting nanoscale particles". In environmental nanotoxicology research, Science of the total environment, vol 772, ISSN00489697.https://doi.org/10.1016/j.scitotenv.2021.145478.

[19] J. E. Batey et al, (2023) "Ultrahigh-Throughput Single-Particle Hyperspectral Imaging of Gold Nanoparticles", Analytical Chemistry, vol 95. https://doi.org/10.1021/acs.analchem.2c05336.

[20] Carolina Blanch et al, (2024) "Hyperspectral microscopy as a particle exposure assessment tool", Proc. SPIE 12848, Three-Dimensional and Multidimensional Microscopy, XXXI, 1284803; https://doi.org/10.1117/12.3002829

[21]https://www.manualslib.com/products/Leica-Dm5000b-3043767.html

[22] Matlab (2019). The Mathworks, Natick. https://mathworks.com.

[23] PerClass BV 2008-2022, Delft, NL. http://perclass.com/perclass-toolbox/product

[24] Naes, T., et al "A User-Friendly Guide to Multivariate Calibration and Classification". NIR Publications (2004).

[25] Gonzalez, R.C & Woods, R.E "Digital Image Processing", Eaglewood Cliffs, NJ: Prentice-Hall, 2002.

[26] Holland, J. H. (1992). Genetic algorithms. Scientific American, 267. https://doi.org/10. 1038/scientificamerican0792-66.